A Crossbar GFET Platform with bioADC Integration for Multiplexed, Energy-Efficient Biosensing

Tyler Andrew Bodily[1], Min Suk Lee[1], Anirudh Ramanathan[2], Akshay Paul[3], Abhijith Karkisaval-Ganapati, Yuchen Xu[3], Oscar Vazquez-Mena[4], Ratnesh Lal[5,1], and Gert Cauwenberghs[6,3]

***Abstract*— We present platform technology consisting of a scalable, low-power graphene field-effect transistor (GFET) array integrated with a custom neural interface system-on-chip (NISoC) for multiplexed biosensing. The platform features a 10×10 GFET crossbar architecture with high-density channel integration and side-gated liquid sensing, enabling simultaneous detection of multiple bioanalytes in a compact footprint. Electrical characterization under varying phosphate-buffered saline (PBS) concentrations confirms stable Dirac point behavior and sensitivity to ionic strength, highlighting the system's electrostatic responsiveness. Integration with a low-power bioADC-based NISoC supports both current- and voltage-clamp operation, achieving sub-µW/channel power consumption. Current-clamp mode offers enhanced energy efficiency, critical for continuous monitoring in wearable applications.**

A streamlined graphene transfer process and dielectric-isolated crossbar design ensure reproducible device performance across the array. The platform is being developed for surface functionalization with DNA aptamers to enable multiplexed biomarker detection in physiological fluids. These advancements position the system for real-time monitoring of health, stress, or disease markers in digital health and athletic performance settings. This work demonstrates a promising direction for next-generation wearable biosensors with low-power, high-density, and real-time signal acquisition capabilities.

***Clinical relevance*— Graphene field-effect transistors (GFET) have significant potential for biological molecule detection. This work builds upon that potential by enabling the simultaneous detection of multiple bioanalytes from a single platform and device.**

I. Introduction

Continuous health monitoring and real-time biomolecular detection are critical for emerging applications in wearable diagnostics, personalized medicine, and athletic performance tracking. Traditional biosensing approaches—such as electrochemical, optical, and lateral flow assays—face limitations in multiplexing, miniaturization, and real-time data acquisition.[1], [2]

[1]Shu-Gien Gene-Lay Department of Bioengineering, University of California San Diego, La Jolla, CA, USA
[2]Department of Material Sciences and Engineering, University of California San Diego, La Jolla, CA, USA
[3]Institute for Neural Computation, University of California San Diego, La Jolla, CA, USA
[4]Department of Chemical and Nanoengineering, University of California San Diego, La Jolla, CA, USA
[5]Department of Mechanical and Aerospace Engineering, University of California San Diego, La Jolla, CA, USA
[6]Department of Electrical Engineering and Bioengineering, University of California San Diego, La Jolla, CA, USA

Graphene field-effect transistors (GFETs) offer unique advantages as biosensing platforms due to their high carrier mobility, large surface-to-volume ratio, and sensitivity to electrostatic surface changes.[2], [3], [4], [5] The surface area of graphene can readily be modulated with biomolecular probes such as antibodies or ssDNA aptamers improving the selectivity of the biosensor.[6], [7] Single-channel GFET biosensors have successfully detected a wide range of analytes, including viral particles, amyloid-beta, and tau proteins.[8], [9], [10] However, their application in scalable, low-power, and high-density systems for wearable use remains underdeveloped.

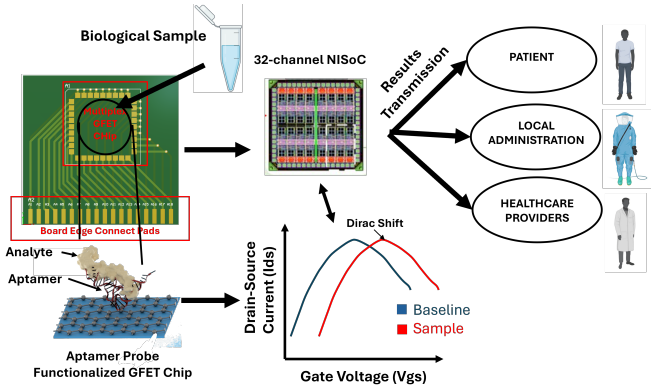

Fig. 1. Schematic of the GFET biosensing workflow. Biological samples introduced into the microfluidic channel interact with DNA aptamer-functionalized graphene channels. Target analyte binding induces a shift in surface potential, modulating the Dirac point. The NISoC chip performs voltage measurements across each GFET while sweeping the gate voltage to detect analyte-induced changes in channel conductance.

In this work, we present a 10×10 multiplexed GFET crossbar array integrated with a custom low-power neural interface system-on-chip (NISoC) for real-time, energy-efficient biosensing.[11] The system enables current- and voltage-clamp operation at sub-microwatt power levels, and supports future functionalization with DNA aptamers for selective and simultaneous detection of multiple biological targets (Fig. 1). Early validation includes clean graphene transfer, stable Dirac behavior under ionic modulation, and low cross-talk between array elements.

These results demonstrate a scalable biosensing platform suitable for integration into compact, wearable systems for health, wellness, and performance monitoring.[12] The following sections detail the fabrication, characterization, and performance of the GFET array and its integration with the

NISoC.

II. Methods

A. Design Specifications

To enable high-density multiplexed biosensing, a crossbar architecture was implemented using 32 individual NISoC readout channels. This design maximizes array density by separating source and drain traces onto different metal layers, insulated by an intermediate dielectric layer (Fig.2). The GFET channels are gated using a side-gate (liquid-gate) configuration to simplify fabrication.

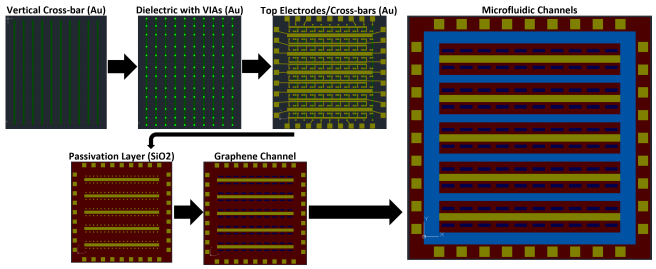

Fig. 2. Layout of the GFET crossbar array consisting of 10×10 individually addressable biosensors. The array is organized into five independent gate electrodes, each connected to two rows. Key fabrication steps include patterning of the source and drain crossbars, PECVD dielectric deposition, gate electrode formation, SiO_2 passivation, graphene transfer and etching, and integration of the microfluidic channel.

B. Crossbar Array Fabrication

Fabrication was performed on 4-inch Si wafers with 300 nm thermally grown SiO_2 (see Fig. 3 for illustration). The process began with spin-coating a bilayer liftoff resist: 400 nm PMGI followed by 2µm positive photoresist. Features for the source metal layer—including contact pads and crossbars—were patterned using a maskless aligner. A 10 nm Cr / 100 nm Au layer was deposited via e-beam evaporation, followed by liftoff.

A plasma-enhanced chemical vapor deposition (PECVD)-deposited dielectric stack (250 nm SiO_2, 100 nm SiNx, and 250 nm SiO_2) was used to electrically isolate the metal layers and reduce pinhole defects. Vias were defined via dry etching to expose the underlying contacts.[13] A second metal deposition step added the drain/gate layer and final contact pads using 300 nm Au. To protect metal traces from electrolyte exposure during biosensing, a 400 nm SiO_2 passivation layer was deposited, leaving only the graphene channels and gate electrodes exposed.[7] The wafer was then diced into individual chips and prepared for graphene integration.

C. Graphene Wet Transfer Protocol

Clean and reproducible graphene channels are essential to the device's sensitivity. A wet-transfer approach was used to transport the graphene from the CVD grown copper substrate to the desired array platform. The desired chip size was cut from the Copper/graphene/polymethyl methacrylate (PMMA) substrate (Graphenea) and placed, copper-side down in .7M ammonium persulfate solution (APS)

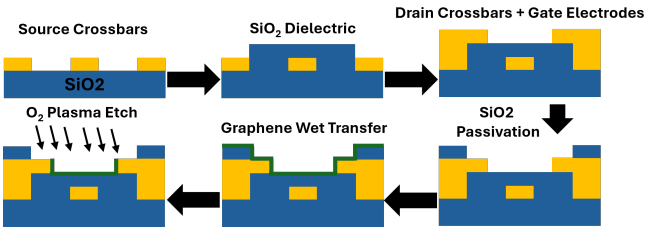

Fig. 3. Fabrication flow for the GFET crossbar array. Key steps include source trace patterning via photolithography, PECVD-based dielectric stack deposition, drain and gate metallization, SiO_2 passivation to protect metal layers, and final graphene transfer and channel definition via oxygen plasma etching.

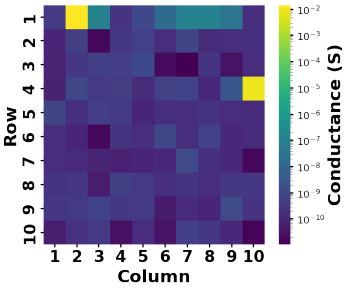

4. Heatmap of conductance between crossbar rows and columns measured at 100 mV bias. Yellow regions indicate low-resistance shorts (100 Ω), while dark regions indicate negligible leakage. Over 98% of crossbar pairs exhibit proper dielectric isolation, confirming crossbar integrity.

and allowed to etch the copper away for 5 hours. The graphene/PMMA stack was transferred to deioinized (DI) water and cleansed of salt residue for 2 hours then transferred the chip substrate. The graphene/PMMA stack was dried and then several drops of 120k PMMA (Thermoscientific) in chlorobenzene was deposited on the graphene/PMMA stack (50 mg/ml). This dissolves the PMMA on the graphene and allows the wrinkles and folds in the graphene that occur throughout the transfer process to relax.[14] The PMMA was recured overnight and then the substrate was baked on a hotplate at 130 C for 2 hours before acetone rinse and overnight acetone bath to remove the PMMA coating.

The graphene channel was etched by using a 400 μm PMGI resist protective layer and patterning the channels. The exposed region was etched by a reactive-ion etcher (RIE) that produces O_2 plasma.

III. Results

A. Crossbar Validation

A series of conductance measurements was conducted to validate the success of crossbar isolation and the insulation of the dielectric layer. This was done by measuring the conductance between the drain, source, and gate pads consecutively. The results indicate negligible conductance between crossbars over the majority of the array (98%) with a few 100 ohm regions affected by pinhole shorts (Fig. 4). The leakage current from the gate to source channels is orders of magnitude larger than the current across the graphene channels (drain-source) after graphene transfer, patterning and etching.

B. GFET Validation

Several iterations of graphene transfer and etching were performed to optimize the graphene purity and uniformity across the channel area. The cleanest and smoothest transferred graphene required several hotplate heating steps prior to PMMA removal, a chlorobenzene dissolution of the PMMA on the graphene/PMMA/substrate stack, and an annealing step post-graphene etching. Raman spectra collected before and after graphene patterning and etching assisted in the optimization of the etching process. Graphene has a peak at 2690 cm^{-1} (2D or G') and 1580 cm^{-1} (G), where the ratio of the 2D/G band intensities indicates the monolayer property of the graphene substrate.[15] Average measurements (8 regions) of the graphene channel region prior to etching are shown in the Table I. An illustration of the Raman spectroscopy locations and results are shown in Fig. 5.

TABLE I
RAMAN SPECTROSCOPY 2D/G RATIO

Location	Pre-Etch	Post-Etch
Channel Region	3.4 ± .7	4.3 ± .6
Outside Channel	3.3 ± .4	1.1 ± .3

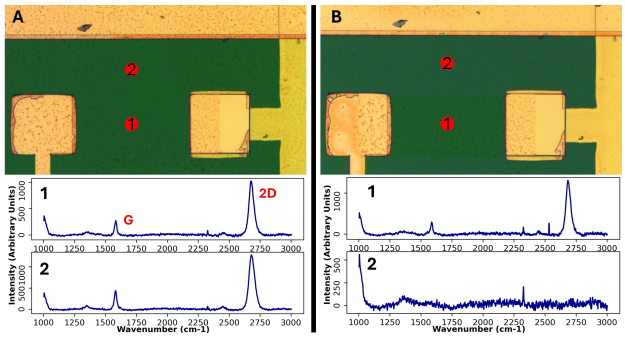

Fig. 5. Raman spectroscopy of graphene channels before and after etching. (A) Graphene following PMMA removal, showing Raman spectra collected from within the channel region (top) and outside the channel (bottom). (B) Corresponding Raman spectra after graphene etching and annealing. The post-etch increase in the 2D/G ratio within the channel confirms successful graphene patterning and monolayer integrity.

C. NISoC-GFET Integration

Initial transfer characteristics were measured using a constant drain–source voltage of 100 mV while sweeping the gate voltage from –1 V to +2 V, following protocols established in prior single-channel GFET studies (Fig.6).[8], [10] Measurements were carried out in liquid-gated situations with varying ionic strength buffers. The observed Dirac points averaged 1.34 V, consistent with previously reported values for p-doped single-channel GFET biosensors.[8] This shift is characteristic of p-type behavior in CVD-grown graphene and reflects charge neutrality under liquid gating conditions.

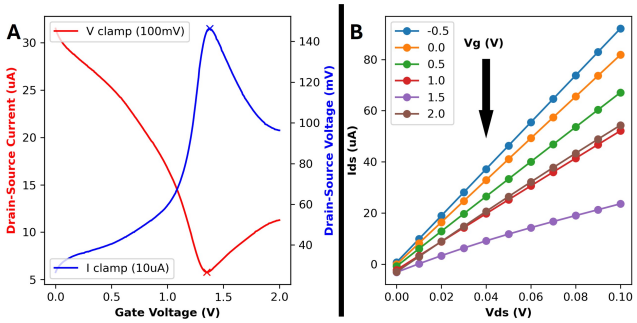

Fig. 6. Electrical characterization of a single GFET biosensor. (A) Transfer curves under voltage-clamp (100 mV) and current-clamp (10 µA) conditions in PBS, showing minimal Dirac point shift (1.35 V vs. 1.37 V). (B) Output characteristics (I_{DS} vs. V_{DS}) under varying gate voltages (V_{GS}), confirming linear response and Ohmic contact behavior.

Fig. 6 illustrates the power consumption benefits of operating the GFET biosensors in current clamp mode. We see a shift in the Dirac point of only 20 mV between the two measurements. The voltage clamp mode has a reduced power at the Dirac point whereas the current clamp offers the greatest power efficiency. As we move further from the Dirac point the device will require less power to produce the same signal sensitivity:

$$V\text{-Clamp: } P = 6.2\mu A \times 100mV = .62\mu W$$

$$I\text{-Clamp: } P = 10\mu A \times 150mV = 1.4\mu W$$

The GFET channels were further characterized by varying the V_{DS} and measuring I_{DS} at different stable values of V_{GS}. We observed Ohmic conductive characteristics which are consistent with a graphene FET with ideal electrode contact Fig. 6B. The overlapping I_{DS} vs V_{DS} at the gate voltages of 1 and 1.5 are representative of being on either side of the charge neutrality point (1.35).The consistency of the Dirac point across the array is illustrated by a simple heat map at 8 different adjacent locations within the GFET array (Fig. 7A). Each was measured using a voltage clamp (100 mV). These consistent Dirac shifts across the array confirm the suitability of the platform for reliable biomarker detection in multiplexed configurations.

The NISoC enables conducting the current-clamp measurement at substantially less power, at supplied currents down to 100 nA, and with measured voltage sensitivity down to 1 μV_{rms}, allowing to conduct continuous GFET sensing with less than 1 μW per channel.

D. Ionic Strength

To evaluate the influence of ionic strength on GFET electrical characteristics, transfer curves were measured in phosphate-buffered saline (PBS) solutions ranging from 0.001× to 1× concentration. A clear shift in the Dirac point was observed as a function of ionic strength: at lower concentrations (0.001×, 0.01× PBS), the Dirac point appeared at higher gate voltages, while higher ionic strengths (0.1× and 1× PBS) resulted in a progressive shift toward lower gate voltages (Fig. 7B). This behavior is attributed to modulation

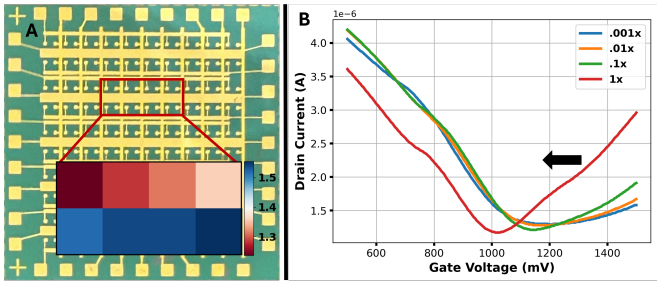

Fig. 7. (A) Spatial mapping of Dirac point voltages across adjacent GFET channels in the multiplexed array under 100 mV voltage clamp. Consistent Dirac points confirm fabrication uniformity and electrostatic stability. (B) Transfer curves under varying PBS ionic strengths (0.001× to 1×), demonstrating a leftward shift in Dirac voltage with increasing ionic concentration due to reduced Debye length and enhanced gate coupling as indicated by the black arrow.

of the electrical double layer (EDL) capacitance at the graphene–electrolyte interface. In dilute solutions, the Debye length increases, reducing the gate coupling efficiency and requiring a higher gate voltage to reach charge neutrality.[16] Conversely, in higher ionic strength conditions, the Debye length shortens, enhancing the electrostatic gating effect and shifting the Dirac point closer to zero.

IV. Discussion

The demonstrated GFET array architecture offers a robust foundation for multiplexed biosensing, combining clean fabrication, electrostatic sensitivity, and compatibility with low-power integrated circuits. The produced GFET array shows ideal characteristics for biosensing technologies illustrated by clean graphene transfer and etching (Fig. 5), conductance measurements validating the dielectric insulation (Fig. 4), and the consistent and accurate transfer function (Fig. 6). The application of current clamp sensing indicates an increase in power consumption at the Dirac point and a reduction in power use in low-signal regimes. The use of the low-power current-clamp modality of the NISoC makes it possible to sample the GFET arrays rapidly in parallel or in succession. The consistency of the Dirac point across the row and column crossbars is encouraging for the reproducibility of biosensor results (Fig. 7A). PBS ionic strength experiments show predictable transfer function characteristics (Fig. 7B). By modulating the surface of the sensor with varying ion-selective membranes future work will explore the arrays ability to quantify a wide variety of ions rapidly.

V. Concluding Remarks

The integration of a multiplexed GFET array with a low-power NISoC represents a scalable and energy-efficient platform for real-time biosensing. Building on previous single-channel GFET biosensor designs, this work demonstrates an optimized graphene transfer methodology and stable device behavior under current-clamp operation. The compact footprint and low power consumption of the NISoC, coupled with the high-density GFET array, make the system well-suited for wearable health monitoring and digital wellness applications.

Ongoing efforts focus on improving device yield and uniformity, and on implementing selective functionalization of individual GFET channels with DNA aptamers for multiplexed biomarker detection. This will enable simultaneous quantification of multiple protein targets relevant to physiological stress, illness, or performance in athletic settings. The platform is being integrated into a compact PCB for future deployment in wearable or point-of-care diagnostics., paving the way for applications in personalized medicine, continuous health monitoring, and wearable biotechnology.

Acknowledgments

The authors would like to thank the Interfaces Graduate Training Program at UCSD (NIH T32 training grant), the Nano3 Cleanroom (Qualcomm Institute, UCSD) for expertise in nanofabrication and state of the art equipment, and members of the Integrated Systems Neuroengineering Lab (ISNL, UCSD).

References

[1] K. Curtin, et al., Recent Advances in Digital Biosensing Technology, *Biosensors*, 673, 2022
[2] H. W. Lu, et al., The promise of graphene-based transistors for democratizing Multiomics Studies, *Biosensors and Bioelectronics*, 195, 113605, 2022
[3] C. Andronescu, et al., Graphene-based field effect transistors as biosensors, *Current Opinion in Electrochemistry*, 3, 11–1, 2017
[4] J. H. Lee, et al., Electrical property of graphene and its application to electrochemical biosensing, 9, 297, 2019
[5] A. K. Geim, K. S. Novoselov, The Rise of Graphene, *Nature Materials*, 183-191, 2007
[6] S. Wang, et al., Recent Advances in Graphene-Based Field-Effect Transistor Biosensors: A Review on Biosensor Designing Strategy, *Journal of Electrochemical Society*, 169, 2022
[7] M. Hinnemo, et al., Protein sensing beyond the Debye length using graphene field-effect transistors. *IEEE Sensors Journal*, 18(16), 6497–6503, 2018
[8] D. K. Ban, et al., Rapid self-test of unprocessed viruses of SARS-CoV-2 and its variants in saliva by portable wireless graphene biosensor, *PNAS*, vol. 119, 28, 2022
[9] A. Beroud, et al., Graphene field-effect transistors as bioanalytical sensors: design, operation and performance, *Analyst*, 146, 2021
[10] T. A. Bodily, et al., In pursuit of degenerative brain disease diagnosis: Dementia biomarkers detected by DNA aptamer-attached portable graphene biosensor, *PNAS*, 120, 47, 2023
[11] A. Paul, et al., Neural recording analog front-end noise reduction with digital correlated double sampling, *2022 IEEE Biomedical Circuits and Systems Conference (BioCAS)*, 2022
[12] T. Nguyen, et al., Field Effect Transistor Based Wearable Biosensors for Healthcare Monitoring, *Journal of Nanobiotechnology*, 24, 411, 2023
[13] V. B. Juska, et al., Silicon microfabrication technologies for biology integrated advance devices and interfaces. *Biosensors and Bioelectronics*, 237, 115503, 2023
[14] S. Krause, et al., Graphene-on-Glass preparation and cleaning methods characterized by single-molecule DNA origami fluorescent probes and raman spectroscopy, *ACS Nano*, 15, 6430-6438, 2021
[15] L. M. Malard, et al., Raman spectroscopy in graphene, *Physics Reports*, 473, 51-87, 2009
[16] A. Purwidyantri, et al., Influence of the Electrolyte Salt Concentration on DNA Detection with Graphene Transistors, *Biosensors (Basel)*, 11, 24, 2021